



## Investigation of Reinforced Particulate Flow and Distribution during Stirring Preparation of A356/SiCp with Experiment and Multi-phase Flow Simulation

X. Shen<sup>1</sup>, F. Sun<sup>2</sup> and H. Zhao<sup>1†</sup>

<sup>1</sup> *National Engineering Research Center of Near-net-shape Forming for Metallic Materials, South China University of Technology, Guangzhou, China*

<sup>2</sup> *Department of Mechanical Engineering, Imperial College London, Exhibition Road, London SW7 2AZ, UK*

† *Corresponding Author Email: hdzhao@scut.edu.cn*

(Received March 5, 2019; accepted July 20, 2019)

### ABSTRACT

Particulate-reinforced aluminum matrix composites produced by stirring casting method exhibit many advantages and are usually used in practical industries. The particulate flow and distribution during the stirring have significant effects on composite casting properties and performances. In this investigation, to study the effect of stirring parameters on particulate distribution, an experimental quenching apparatus was designed, and then A356/50 $\mu$ mSiCp prepared with different stirring speeds and positions were carried out. The particulate fractions at different locations of the prepared composites were quantitatively measured with micro-image analysis, and the charts of particulate distribution along axial directions were summarized and analyzed. Based on liquid-solid multiphase flow theory and multiple rotating reference frame models, a mathematical model of particulate-reinforced aluminum matrix composites stirring process established with consideration of relative flow between liquid and solid particle phases was applied to the experimental composite preparation. By comparing the simulation and experimental results, the effect of stirring condition on the composite slurry and particulate flow as well as the final particulate distribution were analyzed. The comparison shows that the simulated particle distribution exhibits well agreement with the experiment, indicating the validity and exactitude of the established model and method for actual composite stirring preparation. The study shows that low position of impeller would force more particles at the bottom region to flow with composite slurry, improving the particle distribution, and that high stirring speed can cause strong centrifugal force and radial flow of both composite slurry and particles, decreasing the particle uniformity in the composites.

**Keywords:** A356/SiCp; Particulate flow and distribution; Stirring preparation; Liquid quenching; Multiphase flow simulation.

### NOMENCLATURE

$C_{1\epsilon}$	constant in the standard k- $\epsilon$ model	$p$	pressure
$C_{2\epsilon}$	constant in the standard k- $\epsilon$ model	$Re$	Reynolds Number
$C_0$	average of all the values of $C_i$	$r$	radial distance from the central axis of the sample; radial coordinate
$C_i$	mean particulate fraction	$t$	Time
$c_j$	mass fraction for any phase(j)	$U$	radial velocity components
$C_v$	volume fraction of the particle	$V$	angular velocity components,
$d$	diameter of the container	$\vec{v}$	velocity vector
$D$	diameter of the coverage of the stirring blade	$W$	axial velocity components
$F_b$	body force	$z$	axial coordinate
$G$	turbulent kinetic energy production	$\rho_f$	density of the fluid phase
$H$	height from the bottom of the sample	$\rho_j$	density of the phase j
$k$	turbulent kinetic energy	$\rho_m$	density of the mixture
$m$	number of phases	$\rho_p$	density of the particle
$n$	rotational speed		

$\alpha_j$	volume fraction of phase $j$	$\vec{v}_p$	velocity of secondary phase (p)
$\mu_f$	viscosity of fluid phase	$\vec{v}_q$	velocity of primary phase (q)
$\mu_m$	viscosity of the mixture	$\vec{v}_{dr,j}$	drift velocity for secondary phase $j$
$\varepsilon$	dissipation rate of the turbulent kinetic energy	$\theta$	angular coordinate
$\vec{v}_m$	mass-averaged velocity	$\nu_e$	effective viscosity
$\vec{v}_{pq}$	relative velocity of secondary phase (p) and primary phase (q)	$\nu_t$	turbulent viscosity
$\vec{g}$	acceleration of gravity	$\sigma_k$	constant in the standard k- $\varepsilon$ model
		$\sigma_\varepsilon$	constant in the standard k- $\varepsilon$ model

## 1. INTRODUCTION

Composites of Al/SiC<sub>p</sub> exhibit many combined advantages over monolithic metal alloys, including high specific strength, elastic modulus, stiffness and enhanced wear resistances (Chandrasekhar *et al.*, 2018). Precision casting is identified as a promising method in the mass production of Al/SiC<sub>p</sub> components with complex shapes or large volumes for its industrial feasibility, production capacity and cost efficiency.

Basically, castings of Al/SiC<sub>p</sub> are very susceptible to internal particle clusters or particle segregations, since these defects usually provide potential sites for crack formation which lead to catastrophic consequences (Sijo *et al.*, 2016; Prangnell P. B. *et al.*, 1996; Pan *et al.*, 2017). Therefore except for some special situations desiring metal matrix composite (MMCs) with inhomogeneous particulate distribution, e.g. gradient material (Szafran *et al.*, 2007), in most cases a homogeneous distribution of particulates is desired.

Usually reinforced particulates and molten fluid have different contact angles, hence poorly wet particulates are prone to cluster whilst completely wet particulates may tend to sink depending on the density of the ceramic material. Particle cluster and particle segregation always arise spontaneously in Al/SiC<sub>p</sub> after SiC particulates contact with molten aluminum (Hashim *et al.*, 2001). In order to diminish the generation of particle clusters or particle segregation in slurry and to facilitate transferring the particulates into the liquid metal, mechanical stirring is intentionally introduced to the preparation of composite slurry (Hashim J. *et al.*, 1999; Hashim *et al.*, 2002). However, the introduction of stirring leads to particulate distributing non-uniformly through the slurry. Therefore, how to correlate particulate distribution to stirring factors became a new concern during the past decades. Hashim used versatile methods to study the effects of particulate wettability (Hashim *et al.*, 2001), stir geometry (Hashim *et al.*, 1999) and stirring parameters (Hashim *et al.*, 2002) on particulate distribution during stirring.

Great improvements have been achieved in the multiphase flow simulation of SiC<sub>p</sub>/Al composite. Monaghan (Monaghan *et al.*, 1998) built the

program to model the micromechanics associated with the machining of SiC<sub>p</sub>/Al composite. The macro-scale simulation of the cutting process was established with GORGE2, an elastic-visco plastic finite element analysis (FEA) code, and the micromechanical submodel was established by using ANSYS, an elasto-plastic FEA code. The model could describe the material flow, tool wear, failure of the interface between the SiC particles and aluminum matrix, and surface residual stress. Naher (Naher *et al.*, 2007) employed numerical simulation based on software Mixsim to analyze particulate distribution and suspending time in liquid.

Although great improvements have been achieved during past decades, there are still big challenges posing the study of stirring preparation of MMCs. First, most of the previous studies are based on the analysis of flow patterns in transparency liquid, e.g. water, glycerol, etc., for observational accessibility (Hashim *et al.*, 2002; Naher *et al.*, 2007), which ignored the natural difference between the raw material in production and the substituted ones. Second, the previous studies (Naher *et al.*, 2007; Prabu *et al.*, 2006; Sahin *et al.*, 2003) chose different combinations of stirring parameters to fabricate composite slurry depending on the varied geometries of stir, yielding to inevitable misunderstanding in directing the stirring preparation. Third, most of the numerical simulations used to visualize the flow movement during stirring are based on the theory of single phase (Hashim *et al.*, 2002) which doesn't take the multi-reaction between matrix and particulates into account.

In order to advance the understanding and to overcome the above limitations in the study of stirring preparation of MMCs, this paper carried out the investigation of particulate movement during stirring. Liquid quenching technique was employed to prepare composite slurry with different combinations of stirring parameters. The SiC contents in different casting locations were quantitatively measured and analyzed. In addition, the numerical simulation based on Eulerian multiphase theory was performed to investigate the particulate movement during stirring and the performance was validated by comparing the experimental and simulated results.

## 2. EXPERIMENT

### 2.1 Experiment Setup

In order to maintain the original particulate distribution after stirring, it is necessary to cool the slurry as fast as possible after stirring with consideration of diminishing the influences from particulate settling (Vugt *et al.*, 2000) and reaction between the particulates and the dendrites during solidification (Uhlmann *et al.*, 1964; Stefanescu *et al.*, 1988). In this study, an experimental quench apparatus shown in Fig. 1 was designed, which provided an effective method to prepare the PMMCs slurry and cool it rapidly after stirring.

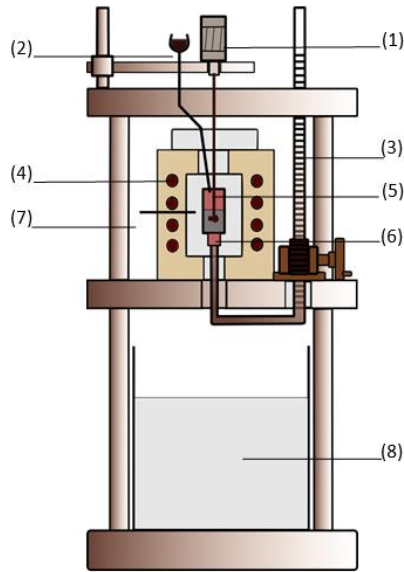


**Fig. 1. Experimental quench apparatus for stirring castings of particulate reinforced metal matrix composites, (1) motor, (2) SiC particulates, (3) lift mechanism, (4) melting furnace, (5) stirring blade, (6) composite slurry, (7) thermal couple (8) cooling medium**

The container with a diameter of 50 mm was produced with stainless steel in order to avoid the split during quenching as well as the corrosion at high temperature during stirring. The impeller having three blades tilted 60° with respect to the horizontal plane was designed based on the studies conducted by Naher *et al.* (Naher *et al.*, 2007), with a diameter of 30 mm. The lift device in the apparatus had a capability of transferring the container to the water within 1.5 seconds.

### 2.2 Experiment Procedure

In this study, A356 (Si 6.5-7.5 wt.%, Mg 0.3-0.45 wt.%, Zn 0.1 wt.%, Fe 0.15 wt.%, Mn 0.1 wt.%, Cu 0.2 wt.%, Ti 0.2 wt.%, Al balance) reinforced by SiC particulates (averaged size of 50 μm) were produced using the experimental quenching apparatus. Prior to the experiments, the SiC particulates were cleaned ultrasonically in an ethanol bath and dried in a vacuum atmosphere, then heated at 900 °C for 6 hours in air to generate

SiO<sub>2</sub> layers on surfaces, which can promote the wettability between the SiC particulates and the molten A356 (Hashim *et al.*, 2001; Bindumadhavan *et al.*, 2001). According to our previous work (Hu *et al.*, 2016), the stirring preparation proceeded step 1 to 4,

- (1) Melting the A356 (275 g) into liquid completely at 730 °C, and then cooling it till the liquidus temperature (610 °C).
- (2) Submerging the steel impeller 20 mm below the liquid surface and rotating it at 300 rpm to generate a stable vortex and adding SiC particles (48 g) into the root of the vortex gradually. After the adding of particulates, heating the slurry to 700 °C gradually with continuously stirring.
- (3) Stirring the composite slurry according to the parameters listed in Table 1 for 20 minutes once the temperature reached 700 °C
- (4) Manipulation of the lift mechanism and quenching the crucible into the water to cool the composite slurry rapidly after the stirring.

In this study, the stirring temperature was chosen around 700 °C based on a compromise consideration: higher stirring temperature would aggravate detrimental chemical reactions between aluminum and SiC (Hashim *et al.*, 2002) and gas entrapment while lower stirring temperature decreases the stirring efficiency and weakens the capability of molding filling as well during industrial producing. For convenience in description, the impeller rotated at a speed of 150 rpm and at a position of H=10 mm is hereafter defined as S150rpm/H10mm, and the same for others in this paper.

**Table 1 Experimental design of A356/SiCp stirring preparation**

NO.	Stirring speed	Stirring position*
1	--	--
2	150 rpm	10 mm
3	150 rpm	5 mm
4	450 rpm	5 mm

### 2.3 Experiment Results

The obtained composite castings were symmetric with respect to the central axis, with a similar height of 60 mm and a diameter of 50 mm. Since the castings have symmetric geometries, half of the plane of symmetry in each casting was ground sequentially with 600, 1000, 1500 and 2000 grit silicon carbide papers and polished with 3 and 1 μm diamond paste. Figure 2 displays the macro-photographs of the polished samples. It is evident that the stirring can homogenize the particle distribution during preparation. There is a particle segregation in the sample without stirring (as Fig. 2(a)), with most of the particulates sinking in the lower part, but samples prepared with stirrings in

Figs. 2(b), (c), (d) had more particulate dispersed through the whole volumes.

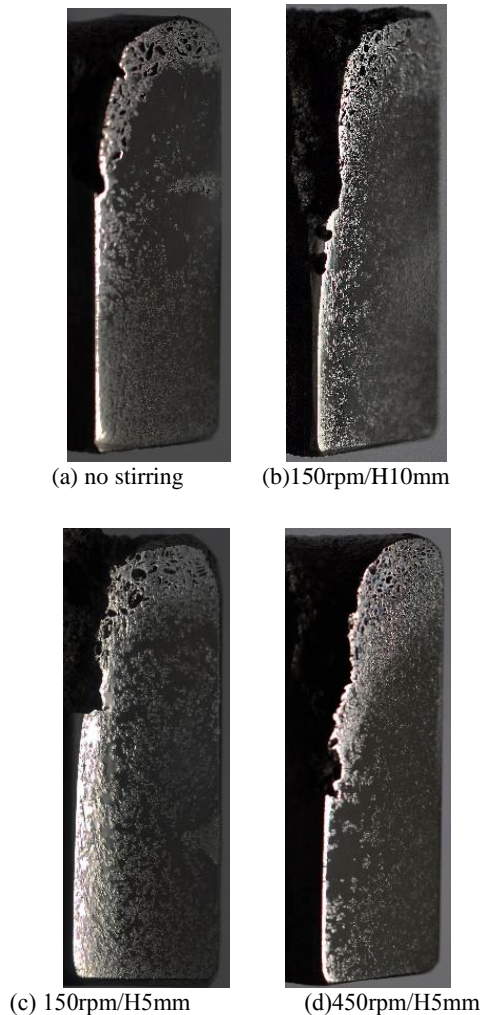


**Fig. 2. Macro photographs of the selected sections.**

Figure 3 shows the metallographs of the samples taken with Leica DMI5000M microscope, in which it can be found that the particulates with irregular shapes had good connection with the A356 matrix. Although it is a common phenomenon that the composite castings are always associated with large porosity resulted from the entrapped gas during stirring (Prabu *et al.*, 2006), there were only few pores in these samples, as shown in Fig. 3. It indicates the validity of transferring particles from the fluid surface into the semi-solid melt with mechanical stirring.

In order to analyze the particulate distribution during the stirring, a quantitative method was employed. In each sample, locations of  $r=5, 12.5$  and  $20$  mm ( $r$  is the radial distance from the central axis of the sample) at different  $H=5, 10, 15, 20, 25, 30$  and  $35$  mm ( $H$  is the height from the bottom of the sample) were marked for the image analysis. At each location, over three metallurgical photos were taken from different micro-fields to obtain the mean

particulate fraction (recorded as  $C_i$ ), and the particulate contents on the images were quantitatively calculated with Image-Pro Plus program.

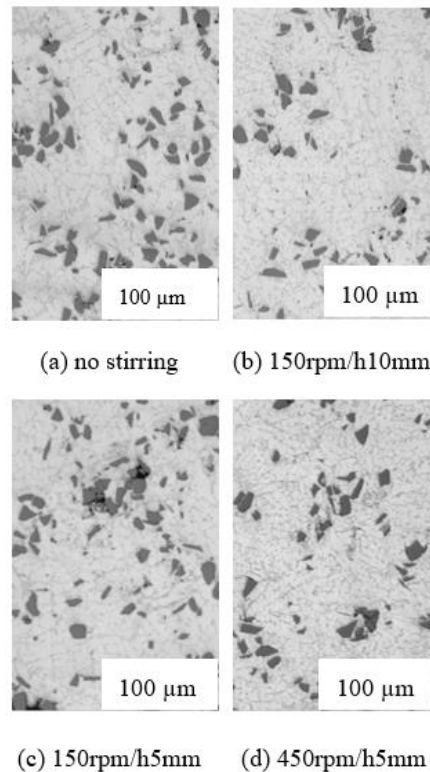


**Fig. 3. Metallographs of the prepared A356/50µmSiCp castings.**

Figure 4 plots the extent of particulate concentration along the height in each sample, in which  $C_0$  is the average of all the values of  $C_i$ . Figure 4(a) indicates that the particulate distributed non-uniformly in the composite slurry of no stirring, with a gradient of particle concentration developed, which is consistent with the results shown in Fig. 2(a). As for composite slurries with specific stirrings, particulate distribution became more uniform as shown in Figs. 4(b) and (c). In addition, by comparing data in Fig. 4(b) and Fig. 4(c), except for the values marked by the circles (invalid values), it is found that the 150rpm/H5mm stirring is more prominent than 150rpm/H10mm stirring in the preparation of composite slurry. Figure 4(d) demonstrates evident signs of particle segregation, with much particulates dispersing in periphery whereas less in center, and it can be identified from Fig. 2(d) as well.

### 3. NUMERICAL SIMULATION

In this experiment, particle phase and matrix phase coexisted during the stirring preparation. Since the particulate fraction was less than 10%, the composite slurry could be regarded as a Newtonian fluid (Saleh, 2004). Even the particle phase is dispersed in physical state, but it can be regarded as a continuum in the prospective of Eulerian method.

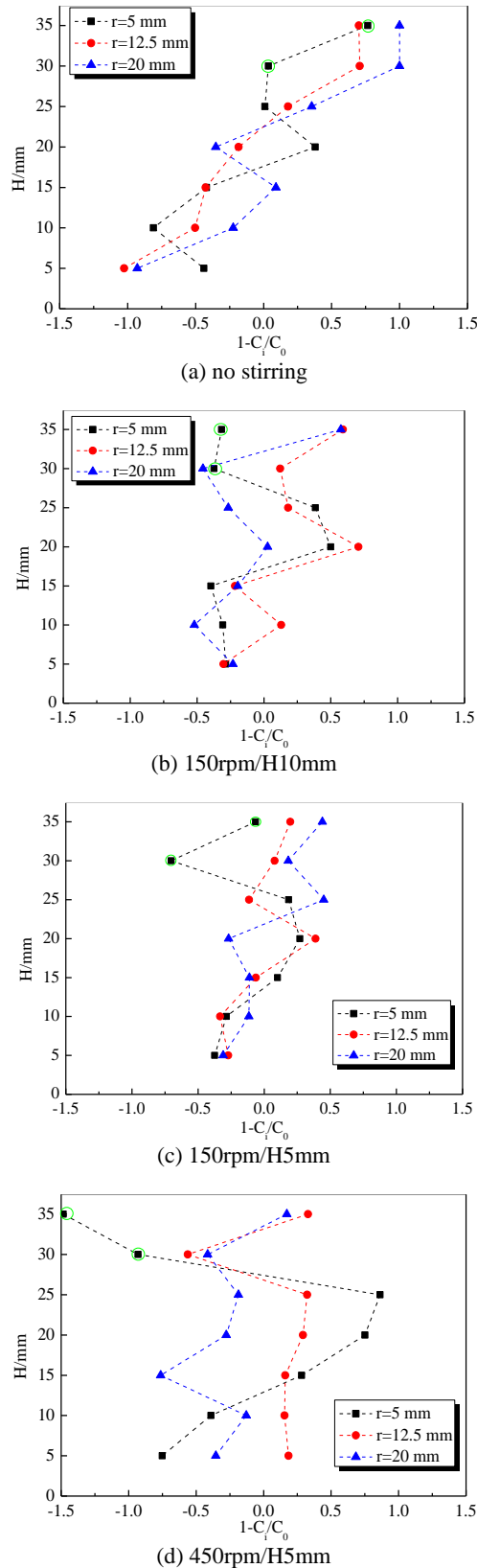


**Fig. 4. Particulate fractions along axial direction in A356/50 $\mu$ mSiC<sub>p</sub>**

### 3.1 Mathematical Model

According to the study by Naher (Naher *et al.*, 2007), it is found that increasing the stirring time

doesn't transform the particulate distribution so much once the stirring time reaches the critical dispersion time (usually less than 180 s) in complete composite slurry. Therefore, it is reasonable to believe that the composite slurry will step into a steady state after stirring time of about 20 minutes. For the composite preparation, uniform distributed particles in the stirring slurry are very wanted. So the purpose of the simulation is to study the final particle distribution in the slurry and to understand effect of stirring parameters on the distribution. Therefore, the steady state of stirring was chosen as the simulation object. Since the SiC particles and Al alloys were heated and molten from the room temperature and the stirring was performed in the constant temperature 750 $^{\circ}$ C, so the heat transfer calculation is not necessary.

The discrete phase (solid phase) is continuous in space, and the liquid and solid phases in the melt can be regarded as interpenetrating fluids moving at different velocities. By solving the existing Navier-Stokes equations, the separate calculation of liquid and solid phases can be realized.

The main controlling equations employed to describe the flow characteristics of A356/SiC<sub>p</sub>, such as continuity equation, momentum equation, relative velocity and fraction equation, were solved within the Multiple Reference Frame (Issa *et al.*, 1994) embodied in FLUENT using the steady-state iterative algorithm.

$$\frac{\partial}{\partial t}(\rho_m) + \nabla \cdot (\rho_m \vec{v}_m) = 0 \quad (1)$$

$$\vec{v}_m = \frac{\sum_{k=1}^n \alpha_j \rho_j \vec{v}_j}{\rho_m} \quad (2)$$

$$\rho_m = \sum_{k=1}^n \alpha_j \rho_j \quad (3)$$

Momentum equation

$$\frac{\partial}{\partial t}(\rho_m \vec{v}_m) + \nabla \cdot (\rho_m \vec{v}_m \vec{v}_m) = -\nabla p + \nabla \cdot \left[ \mu_m (\nabla \vec{v}_m + \nabla \vec{v}_m^T) \right] + \rho_m \vec{g} + \vec{F} + \nabla \cdot \left( \sum_{j=1}^n \alpha_j \rho_j \vec{v}_{dr,j} \vec{v}_{dr,j} \right) \quad (4)$$

$$\mu_m = \sum_{j=1}^n \alpha_j \mu_j \quad (5)$$

$$\vec{v}_{dr,j} = \vec{v}_j - \vec{v}_m \quad (6)$$

Slip velocity

The slip velocity is defined as the velocity of a secondary phase (p) relative to the velocity of the primary phase (q). The mass fraction for any phase (j) and the relationship between the drift velocity and the slip velocity are shown by the following expression:

$$\vec{v}_{pq} = \vec{v}_q - \vec{v}_p \quad (7)$$

$$c_j = \frac{\alpha_j \rho_j}{\rho_m} \quad (8)$$

$$\vec{v}_{dr,p} = \vec{v}_{pq} - \sum_{j=1}^n c_j \vec{v}_{qj} \quad (9)$$

The Reynolds number (M. Baccar *et al.*, 1999) is given in the following form:

$$Re = \frac{\rho_m D^2 n}{\mu_m} \quad (10)$$

$$\rho_m = \rho_f (1 - C_v) + \rho_p C_v \quad (11)$$

$$\mu_m = (1 + 2.5C_v) \mu_f \quad (12)$$

$Re$  is calculated to be greater than 10000, which shows that the melt with the minimum stirring speed is a full turbulence, so the  $k-\epsilon$  turbulence model is chosen. In the momentum calculation, standard  $k-\epsilon$  model (Driss Z. *et al.* 2010) was used to consider turbulence.

$$\frac{\partial k}{\partial t} + \text{div} \left[ \vec{V} k - \frac{2}{\pi} \left( \frac{D}{d} \right)^2 \frac{1}{Re} \left( 1 + \frac{v_t}{\sigma_k} \right) \overrightarrow{\text{grad}} \cdot k \right] = \frac{2}{\pi} \left( \frac{d}{D} \right)^2 \frac{1}{Re} G - \epsilon \quad (13)$$

$$\frac{\partial \epsilon}{\partial t} + \text{div} \left[ \vec{V} \epsilon - \frac{2}{\pi} \left( \frac{D}{d} \right)^2 \frac{1}{Re} \left( 1 + \frac{v_t}{\sigma_\epsilon} \right) \overrightarrow{\text{grad}} \cdot \epsilon \right] = \frac{\epsilon}{k} [C_{1\epsilon} \left( \frac{D}{d} \right)^2 \frac{1}{Re} G - C_{2\epsilon} \epsilon] \quad (14)$$

The turbulent kinetic energy production is given in the following form:

$$G = \nu_t \left[ 2 \left[ \left( \frac{\partial U}{\partial r} \right)^2 + \left( \frac{\partial V}{r \partial \theta} + \frac{U}{r} \right)^2 + \left( \frac{\partial W}{\partial z} \right)^2 \right] + \left[ \frac{\partial V}{\partial r} - \frac{V}{r} + \frac{\partial U}{r \partial \theta} \right]^2 + \left[ \frac{\partial W}{r \partial \theta} + \frac{\partial V}{\partial z} \right]^2 + \left[ \frac{\partial U}{\partial z} + \frac{\partial W}{\partial r} \right]^2 \right] \quad (15)$$

The viscosity equations (Bacchar *et al.*, 1999) are given in the following form:

$$\nu_t = C_\mu \frac{\pi}{2} \left( \frac{d}{D} \right)^2 Re \frac{k^2}{\epsilon} \quad (16)$$

The constants of the standard  $k-\epsilon$  model were presented in Table 2.

**Table 2 Standard k-ε model constants.**

$C_{1\epsilon}$	$C_{2\epsilon}$	$C_\mu$	$\sigma_k$	$\sigma_\epsilon$
1.44	1.92	0.09	1.00	1.30

This study applied 3-dimensional grids to represent the different stirring constructions, and approximately 1.3 million triangular cells were meshed for each case. In the simulation, strong stirring zone and convective circulation zone are defined as the moving reference frame zone and the stationary zone respectively, as is shown in Fig. 5. The boundary representing the container wall was defined as a solid and frictionless surface with a constant temperature of 700 °C. The initialization of particulate distributions before stirring were specified according to the experimental particulate fractions in the sample produced without stirring (Fig. 2(a)). Considering the effects of irregular particulate shapes on fluid flow, it set an averaged shape coefficient of 0.6 for the particulates in the simulations (Haider *et al.*, 1989). The whole calculations were performed in a HP Z800 workstation (Intel (R) Xeon (R) CPU, 48G RAM), and the general calculation cost about 150 min for each group.

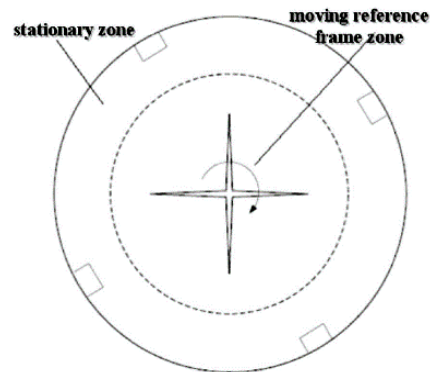


**Fig. 5. Division of computational area for numerical simulation of stirring process.**

### 3.2 Simulation Results

The velocities of molten A356 during stirring preparation are presented in Fig. 6, indicated graphically by velocity vectors. In the horizontal direction, the fluid flowed around the central axis and the velocities varied with respect to the radial positions as well as the vertical positions. Apart from the circular motion in the horizontal direction, the fluid also flowed in the vertical direction apparently, which enables the sank particulates to refloat and suspend. There were two obvious circulation zones above and below the impeller, respectively, taking the right half of Fig. 6 for example. As the impeller began to rotate, the blades would mix and push the nearby fluid to move towards the peripheral area. Once the fluid reached the wall, it divided into two directions and flowed round the circulation zones, and afterwards they were transmitted to the blades for the subsequent circulation.

The profile of the circulation zones in the slurry displays a butterfly pattern. There are two “dead zones” above the upper surface and below the lower surface of the stir, respectively. In Ref (Hashim *et*

*al.*, 2002), Hashim mentioned the dead zone and its effects during the preparation of particle reinforced composites. In this case, the lower dead zone was suppressed due to the bottom container wall while the upper dead zone extended freely in the fluids. In these dead zones, fluids always have very low velocities compared to the fluids near the side wall of the container. Figure 7 displays the particle velocities in the stirring of 150rpm/h10mm, 150rpm/h5mm and 450rpm/h5mm respectively. Different from the velocities of the molten A356 in Fig. 6, the particulates only occupied 3/4 of the longitudinal section approximately, and few particulates dispersed in the top region. Figure 8 shows the particle distribution in the slurry at different stirring parameters. It is obvious the uniformity of the distribution at 150rpm/H5mm is better than those of 150rpm/H10mm and 450rpm/H5mm.

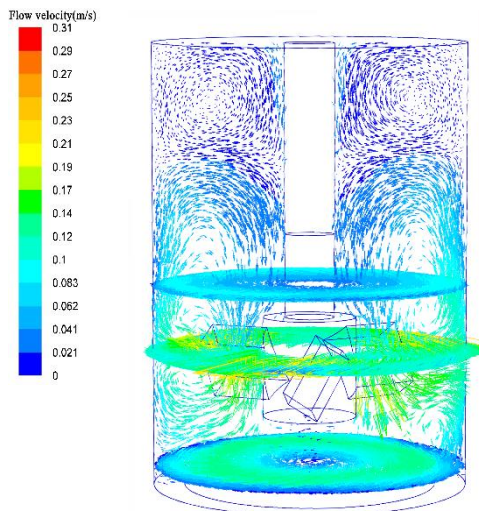
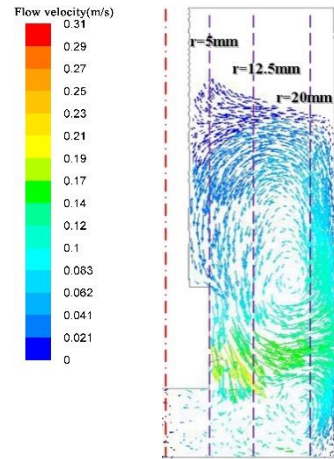


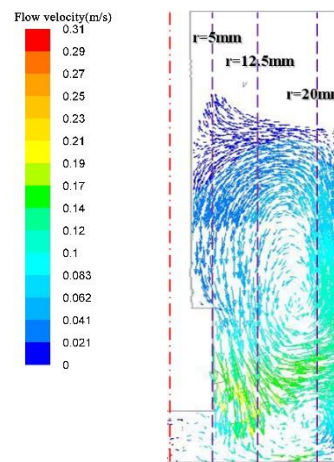
Fig. 6. Flow velocity of molten A356 during stirring preparation.

#### 4. VALIDATION AND DISCUSSION

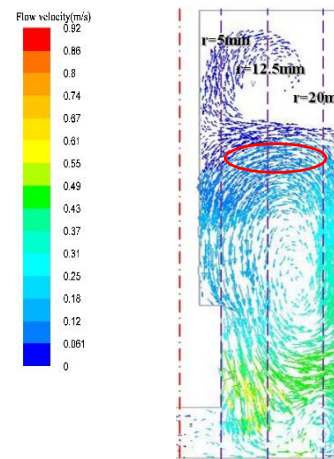
The simulated and experimental results of the final particulate fraction are plotted in the following figures for comparison. In order to aid generalization of interpretation of the experimental and simulated results,  $\xi$  (defined as the ratio of the actual particle volume fraction to the largest fraction, which can be output the simulation results in Fig. 8) was used to represent the relative volume fraction (Mat *et al.*, 2006; Sun *et al.*, 2013; Chen *et al.*, 2015) During the quenching process after the stirring, the shrinkage of the castings happened and a large shrinkage cavity formed in the top-center parts (Fig. 2), indicating the liquid flowing downwards during solidification. Therefore, the experimental results marked by circles were invalid to verify the simulation results there due to the move of particles with the liquid in the shrinkage feeding flow.



(a) 150rpm/H10mm



(b) 150rpm/H5mm



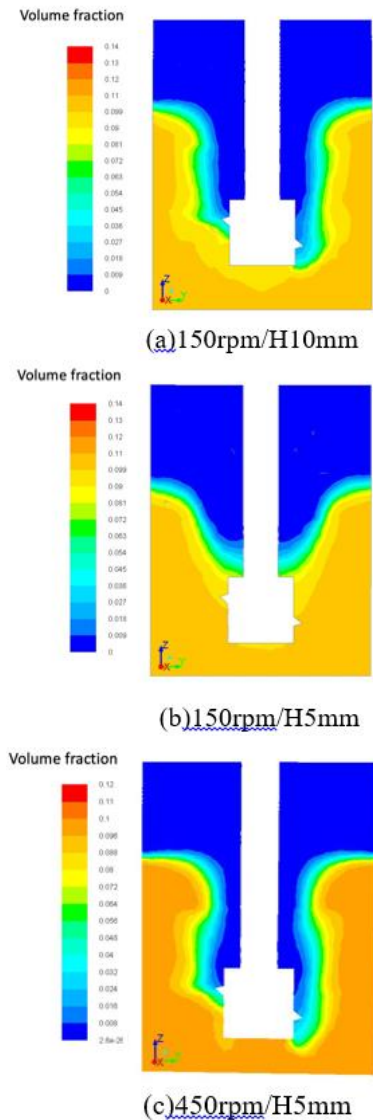
(c) 450rpm/H5mm

Fig. 7. Distribution of SiC particulates velocity during stirring

#### 4.1 150rpm/H10mm Experiment

The experimental and simulated results of particulate distribution during the 150rpm/h10mm stirring is shown in Fig. 9. According to Fig. 7(a), there is no obvious circulation zone in the top one third of the slurry due to the vortex dissipation in

the slurry. Therefore, only few particulates were able to go through this zone while more particulates concentrated in the circulation zone (the lower two thirds of the whole slurry), resulting in a decrease of particulate volume along the height from the bottom of the slurry as indicated in Fig. 9.



**Fig. 8. Distribution of SiC particulates volume fraction during stirring**

From the simulated flow velocities in Fig. 7, only few particulates are able to pass through the upper dead zone above the stir, resulting in a decrease of particle volume from the lower to the upper circulation zones, as Fig. 9(a) indicated. In Fig. 9(b), the particle volumes go through a decline from the lower to the upper circulation zones as well, but it is attributed to the strong centrifugal force generated by the rotating stir. Different from the change of particle volumes in Fig. 9(a), the decrease of particle volumes in Fig. 9(b) displays a ladder-like distribution. In contrast to the particulate distribution in either Figs. 9(a) or (b), the particulates disperse uniformly along height in the

periphery of the circulation zones, revealed in Fig. 9(c). In Fig. 7, the fluid divided into two circulations after it arrived at the side wall and flowed along the side wall, and afterwards the fluid velocity was enlarged (please see the density and value of the flow lines) due to the suppression from the side wall. Therefore, much more particulates circulated through this peripheral region and dispersed in higher positions.

From Fig. 9(a), it is found that the particle volume in the circulation zone varied significantly. The particle volume maintained uniformly in lower circulation zone (region below the rotating stir) whereas it decreased dramatically through upper circulation zone (region above the stir). However, from Figs. 9(a), (b), (c), it is evident that the particles volume tends to be increased and particulates distributed more uniformly along the radius in the upper circulation zone.

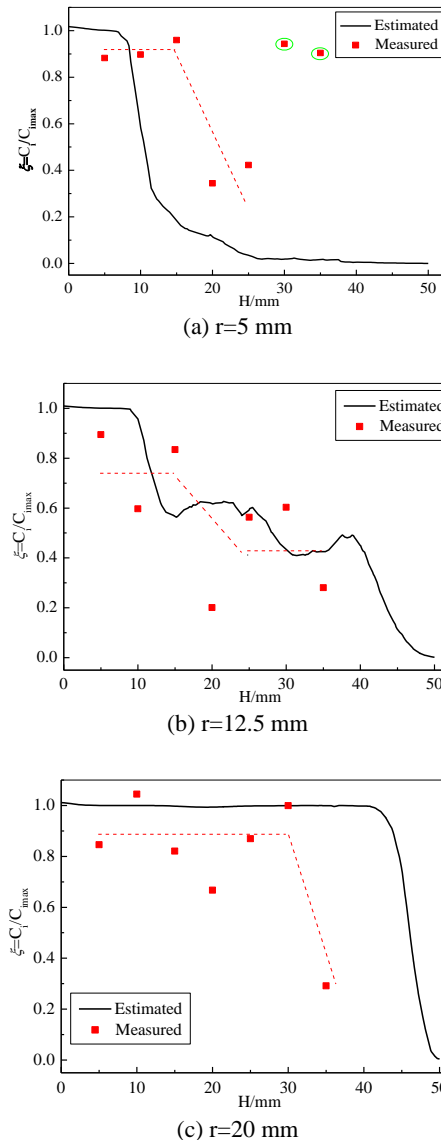


**Fig. 9. Comparison of simulated and experimental results of particulate distribution during 150rpm/h10mm stirring.**

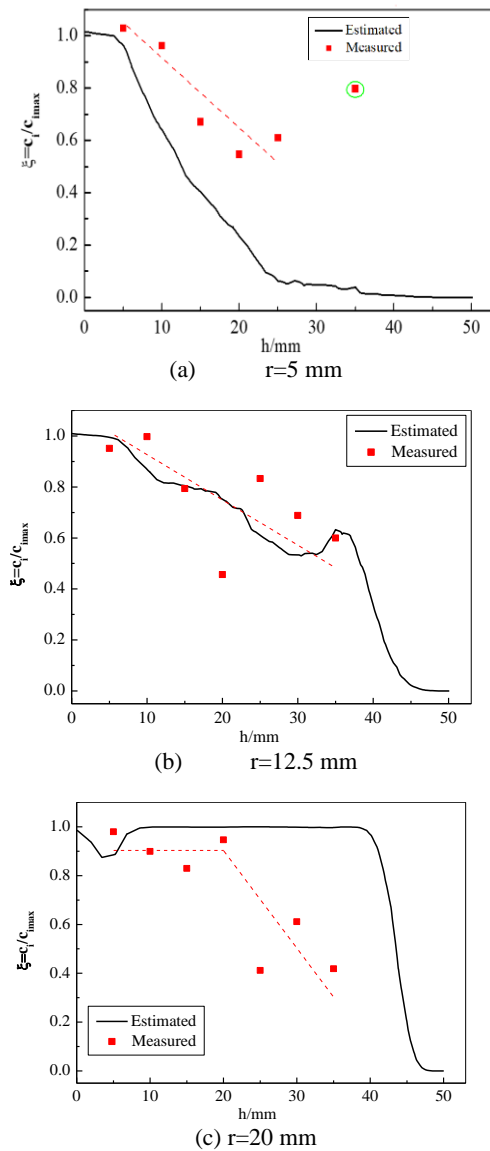


**Fig. 10. Comparison of simulated and experimental results of particulate distribution during 150rpm/h5mm stirring.**

#### 4.2 150rpm/H5mm Experiment

The particulate distribution during 150rpm/h5mm stirring was shown in Fig. 10. By comparing the particle flow velocities during 150rpm/H5mm stirring (Fig. 7(b)) with the 150rpm/H10mm stirring (Fig. 7(a)), it was found that with the decrease of the stir position, the distribution of flow pattern in the slurry seemed to move down as a whole. In addition, as the volume of lower circulation zone below the stir decreased, the density and magnitude of particulate velocities in this region were enlarged. Therefore, the particulates in the base region of the slurry were mixed more strongly and more particulates obtained momentum to flow up and circulate around. The particulate volumes in Fig. 10(a) and (b) show a relatively slower decrease trends compared with the results in Figs. 9(a) and (b). But due to the downwards movement of the flow pattern in the slurry, experimental results in

Fig. 10(c) presented that particulates could not reach the positions as high as 150rpm/H10mm did in Fig. 9(c).

#### 4.3 450rpm/H5mm Experiment

Figure 7(c) displays the particle velocities during 450rpm/H5mm stirring. It was found that the particulate mixed in the composite was intensified, with greater flow velocities (please note the values in the color label) and denser flow lines, the radial flow at the upper boundary of the upper circulation (near H=30 mm and marked by the circle in Fig. 7(c)) was enhanced as well. The comparisons of experimental and simulated distribution of particulates during 450rpm/h5mm stirring were presented in Fig. 11.

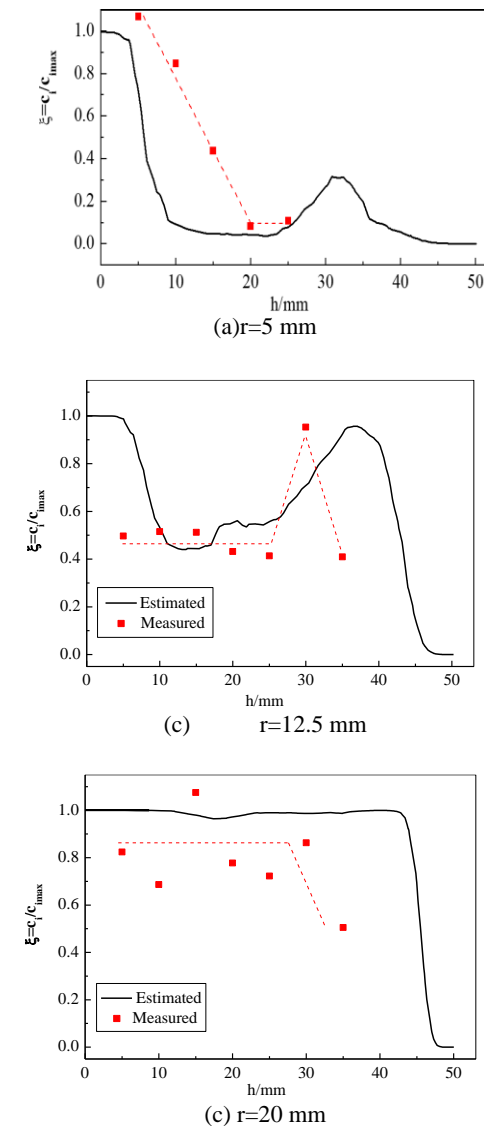


**Fig. 11. Comparison of simulated and experimental results of particulate distribution during 450rpm/h5mm stirring.**

It can be concluded that with the increase of rotating speed, a greater centrifugal force and larger

upper dead zone were generated by the stir. Therefore, the particle volumes near the rotating axis (at  $r=5$  mm) declined dramatically along height from the lower to the upper circulation zone, rapider than the changes in 150rpm/h5mm stirring. In addition, particle volume experienced an increase near the upper boundary of the upper circulation zone ( $H=30$  mm) before maintained low in Fig. 11(a), resulting from the stronger radial flow carrying more particulates. Furthermore, we can find that all the  $r=5$ mm cases (Figs. 9(a), 10(a), 11(a)) are far off the compared test data. What has caused this phenomenon is that the shrinkage of the castings happened during the quenching process after the stirring and a large shrinkage cavity formed in the top-center parts.

In Fig. 11(b), since the radial flow was nearer to the side wall, exhibiting larger velocities compared to the radial flow in Fig. 11(a), more particulates with high momentums flowed through the region from the side wall. Finally, particle volumes in Fig. 11(b) showed a distinct increase near the upper boundary of the upper circulation zone.

In Fig. 11(c), the particulate distribution in the peripheral region displayed a similar trend as 150rpm/h10mm and 150rpm/h5mm showed. But compared to the particulate distribution in the peripheral region under 150rpm/h5mm, more particulates under 450rpm/h5mm were able to obtain higher momentum and dispersed in higher region due to the increase of the rotating speed.

The experiment of 450rpm/h5mm stirring indicates that with a larger rotating speed, the mixing in the base region of the slurry will be enhanced and more particulates there obtain sufficient momentum to flow up. However, there were obvious particle segregations in radial direction in 450rpm/h5mm shown in Fig. 4(d). Actually, the strong centrifugal forces expel amounts of particulates to flow outwards, inducing detrimental particle segregations along radial direction.

In this study, it is found that the 150rpm/h5mm stirring is more prominent compared to 150rpm/h10mm and 450rpm/h5mm combinations, even though the particulates are still unable to distribute uniformly in the upper one third of the slurry during this stirring. Even though a higher stirring speed in the slurry provide the particulates with higher momentum to lift up, an excessive stirring speed probably bring strong centrifugal forces and radial flows, aggravating the particulate distribution and producing particle segregations. The stirring position also has a significant effect on particulate distribution. Lower stirring position will give the particulates in the base region of the slurry more momentum to lift up, but due to the downward movement of the circulation zones, most particulates are unable to disperse in high regions. The above comparison in our study shows that the experimental and simulated results of the particulate distribution are in good agreement apart of few positions. The mathematic model used in this study exhibits huge potential in predicting the particulate distribution during the stirring preparation of

MMCs. The underestimations in the study were possibly caused by the simplification of boundary conditions and particle interactions due to the complication of the multiphase flow.

## 5. CONCLUSION

In this paper, both the experiment and simulation investigation on the effects of stirring speed and position on particulate distribution during A356/SiCp stirring preparation was carried out. The results have shown:

- (1) A liquid quenching apparatus was produced to investigate the particulate distribution. The A356/SiCp slurries prepared with different stirring speeds and positions were conducted and could be quenched rapidly with the apparatus. Hence the particle distributions during the stirring were analyzed.
- (2) The stirring preparation of A356/SiCp was simulated based on the Eulerian multiphase model and multiple reference frames. The simulated results are in good agreement with the experimental results, which confirms the model validity in predicting particulate distribution the composite stirring preparation.
- (3) Low stirring position (h5mm) is able to accelerate more particulates in the bottom region, resulting in their uniform distribution. The low rotating speed (150rpm) can improve the uniformity of particulates with  $50\mu\text{m}$  whereas the higher speed (450rpm) generates stronger centrifugal force and radial flow inducing particle segregation.

## ACKNOWLEDGEMENTS

The research is supported by the projects of National Natural Science Foundation of China (51875211, 50975093) and Guangdong Science and Technology Project (201313090600118).

## REFERENCES

- Baccar, M. and M. S. Abid (1999). Numerical simulation of hydrodynamic and thermal behaviours in a scraped surface heat exchanger operating in turbulent regime. *Revue Générale De Thermique* 38(7), 634-644(11).
- Bindumadhavan, P. N., T. K. Chia, M. Chandrasekaran, H. K. Wah, L. N. Lam and O. Prabhakar (2001). Effect of particle-porosity clusters on tribological behavior of cast aluminum alloy a356-sicp metal matrix composites. *Materials Science & Engineering A (Structural Materials: Properties, Microstructure and Processing)* 315(1-2), 217-226.
- Chandrasekhar P., C. Sudipta and S. Saranjit (2018). Investigation of dynamic effects during cold upset-forging of Silicon Carbide particulate reinforced Aluminium metal matrix

- composite preforms. *Materials Today: Proceedings* 5, 20201-20202.
- Chen F. F. H. D. Zhao, G. Zhu, P. X. Fu, L. J. Xia (2015). Experimental and numerical analysis of flow behavior and particle distribution in A356/SiCp composite casting. *Experimental Thermal and Fluid Science* 68, 39-47.
- Driss, Z., G. Bouzgarrou, W. Chtourou, H. Kchaou and M. S. Abid (2010). Computational studies of the pitched blade turbines design effect on the stirred tank flow characteristics. *European Journal of Mechanics, B/Fluids* 29(3), 236-245.
- Hashim, J., L. Looney and M. S. J. Hashmi (1999). Metal matrix composites: production by the stir casting method. *Journal of Materials Processing Technology* 92-93, 1-7.
- Hashim, J., L. Looney and M. S. J. Hashmi (2002). Particle distribution in cast metal matrix composites—Part I. *Journal of Materials Processing Technology* 123, 251-257.
- Hashim, J., L. Looney and M. S. J. Hashmi (2002). Particle distribution in cast metal matrix composites—Part II. *Journal of Materials Processing Technology* 123, 258-263.
- Hashim, J., L. Looney and M. S. J. Hashmi (2001). The wettability of SiC particles by molten aluminium alloy. *Journal of Materials Processing Technology* 119, 324-328.
- Hu, Q., H. Zhao and F. Li (2016). Effects of Manufacturing Processes on Microstructure and Properties of Al/A356–B4C Composites. *Materials and Manufacturing Processes* 31(10), 1-9.
- Issa, R., J. Y. Luo and D. Gosman (1994). Prediction of Impeller Induced Flows in Mixing Vessels using Multiple Frames of Reference. *European Conference on Mixing, Imech Symposium*.
- Jiang, J. and W. Ying (2015). Microstructure and mechanical properties of the semisolid slurries and rheo-formed component of nano-sized SiC/7075 aluminium matrix composite prepared by ultrasonic-assisted semisolid stirring. *Materials Science & Engineering A* 639, 350-358.
- Mat, M. D. and K. Aldas (2006). Experimental and numerical investigation of effect of particle size on particle distribution in particulate metal matrix composites. *Applied Mathematics and Computation* 177, 300–307.
- Monaghan, J. and D. Brazil. (1998). Modelling the flow processes of a particle reinforced metal matrix composite during machining. *Composites Part A. Applied Science and Manufacturing* 29(1-2), 87-99.
- Naher, S., D. Brabazon and L. Looney (2007). Computational and experimental analysis of particulate distribution during Al-SiC MMC fabrication. *Composites: Part A* 38, 719-729.
- Pan, L., J. Han, Z. Yang, X. Li, J. Wang and Z. Li, *et al.* (2017). Thermal fatigue crack behavior of SiCp/A356 composites prepared by stirring casting. *Results in Physics* 7, 927-933.
- Prabu, S. B., L. Karunamoorthy, S. Kathiresan and B. Mohan (2006). Influence of stirring speed and stirring time on distribution of particles in cast metal matrix composite. *Journal of Materials Processing Technology* 171, 268-273.
- Prabu, S. B., L. Karunamoorthy, S. Kathiresan and B. Mohan (2006). Influence of stirring speed and stirring time on distribution of particles in cast metal matrix composite. *Journal of Materials Processing Technology* 171, 268-273.
- Prangnell, P. B., S. J. Barnes, S. M. Robert and B. Mohan (1996). The effect of particle distribution on damage formation in particulate reinforced metal matrix composites deformed in compression. *Materials Science and Engineering A* 220, 41-56.
- Sahin, Y. (2003). Preparation and some properties of SiC particle reinforced aluminium alloy composite. *Materials and Design* 24, 671-679.
- Saleh, J. M. (2004). *Fluid flow handbook. DENG Dunxia, trans.* Beijing: China Petrochemical Press 212–213.
- Sijo, M. T. and K. R. Jayadevan (2016). Analysis of Stir Cast Aluminium Silicon Carbide Metal Matrix Composite: A Comprehensive Review. *Procedia Technology* 24, 379-385.
- Stefanescu, D. M., B. K. Dhindaw, S. A. and A. Kacar Moitra (1988). Behavior of ceramic particles at the solid-liquid metal interface in metal matrix composites. *Metallurgical Transactions A* 19A, 2847-2855.
- Sun, F. Z., H. D. Zhao, Y. Zhao, P. Y. Dong and F. F. Chen (2013). Flow and distribution of reinforced particulates in A356/SiCp vertical upwards suction casting. *The Chinese Journal of Nonferrous Metals* 23(1), 91-98.
- Szafran, M., K. Konopka, E. K. J. and Bobryk, Kurzydowski (2007). Ceramic matrix composites with gradient concentration of metal particles. *Journal of the European Ceramic Society* 27, 651-654.
- Uhlmann, D. M., B. Chalmers and K. A. Jackson (1964). Interaction between particles and a solid-liquid interface. *Journal of Applied Physics* 35(10), 2986-2991.
- Vugt, L. and L. Froyen (2000). Gravity and temperature effects on particle distribution in Al-Si/SiC composites. *Journal of Materials Technology* 104, 133-144.